Biophysics of the cochlea: Linear approximation

F. Mammano[a)]
International School for Advanced Studies, Strada Costiera 11, 34014 Trieste, Italy

R. Nobili
Dipartimento di Fisica "G. Galilei," Università di Padova, Via Marzolo 8, 35131 Padova, Italy

(Received 18 November 1991; revised 1 December 1992; accepted 17 December 1992)

Several deficiencies affecting previous "box" models of the cochlea are overcome in this paper. Both mechanical and hydrodynamical aspects are treated at a level adequate to the complexity of realistic cochlear structures. The dynamics of the cochlea as a passive physical system, in the linear approximation, is described by an integral equation. It is further shown that this equation describes the properties of the working cochlea, provided a force term that accounts for hair cell motility is included. Numerical solutions for different degrees of outer hair cells activity, obtained by matrix methods in the frequency domain, are presented. Amplitudes and phases of the computer-simulated traveling waves are in fair agreement with basilar membrane responses to tones measured in various experimental conditions.

PACS numbers: 43.64.Kc, 43.64.Bt, 43.64.Ld

INTRODUCTION

Frequency selectivity of the cochlea is determined by the graded elastic properties of the cochlear partition, which are mainly due to the fibers embedded in the basilar membrane (BM). In this paper, the direction of the BM fibers will be referred to as *radial*, whereas that of the coiling axis of the cochlea as *longitudinal*. The direction and the plane orthogonal to the BM will be referred to as *vertical* and *transversal*, respectively. In the following we will mainly refer to the guinea-pig cochlea, which has a trumpetlike longitudinal cross section, as can be inferred from Fig. 1(a) (most of the relevant background material on cochlear anatomy and physiology can be found in Pickles, 1988; and de Boer, 1980, 1984, and 1991).

The organ of Corti is a set of adjacent segments about 10 μm long formed by transversal portions of the cochlear partition and spanning the entire length of the BM. Each segment hosts a triplet of outer hair cells (OHCs) and 0.9 inner hair cells on average (Iurato, 1961). Possessing mass, stiffness, and viscosity, these segments form local oscillators vibrating in transversal planes and longitudinally coupled mainly by the pressure field of the fluid filling the scalae. The relative importance of other coupling terms depends upon the stiffness characteristics of the reticular lamina (RL) and the tectorial membrane (TM), as well as upon the viscosity of the supporting tissues. As the BM displacements at moderate sound-pressure levels (SPLs) are in the range of a few nanometers (Sellick *et al.*, 1982; Robles *et al.*, 1986), elastic longitudinal coupling will be neglected on account of longitudinal flexibility and lack of longitudinal tension of the RL and the TM (see Appendix B). However, longitudinal coupling due to the shearing resistance between adjacent segments of the organ of Corti will be included, as there is no obvious reason to neglect it.

Since the BM displacements are very small, such are also the velocity field of the cochlear fluid and its gradient [about 4×10^{-5} m/s at 10 dB SPL, according to Sellick *et al.* (1982)]. So, in the first part of this paper, the cochlea is described, within the limits of the linear approximation, as a *system of damped oscillators* interacting locally by viscous forces and driven by pressure differences across the BM (*passive cochlea*).

In the second part, the description is expanded to account for recent experimental evidence showing that a physiologically vulnerable mechanism, generally referred to as the "cochlear amplifier," causes the BM to be far more sharply tuned than reported by von Békésy (1960), particularly for near-threshold stimuli (Davis, 1983; de Boer, 1983). The cochlear amplifier is thought to sharpen the resonance of the cochlea by reducing the inherent damping of the cochlear partition (Ashmore, 1987; Pickles, 1988; de Boer, 1991). An indirect evidence that this is indeed the case is probably provided by the existence of cochlear echoes (Kemp, 1978; Wilson, 1980), which seem to indicate that the BM responses to sound *in vivo* occur at the threshold of spontaneous oscillations in a wide frequency range. Hence, in the working cochlea the energy dissipation affecting passive dynamics is almost uniformly neutralized but not overcompensated by the action of the cochlear amplifier (*active cochlea*). The link between cochlear amplifier and OHC motility is examined in Secs. IV and V.

I. PASSIVE COCHLEAR MECHANICS

For the sake of formal clarity, the BM will be described as a continuum rather than a discrete collection of segments. Hence, the segment lengths are regarded as infinitesimal and the local force terms affecting the motion of the BM have the dimension of force per unit length.

Assuming that all such force terms depend linearly on the vertical displacements of the cochlear segments and

[a)]Present address: Department of Physiology, School of Medical Sciences, University Walk, Bristol BS8 1TD, U.K.

 0001-4966/93/063320-13$06.00

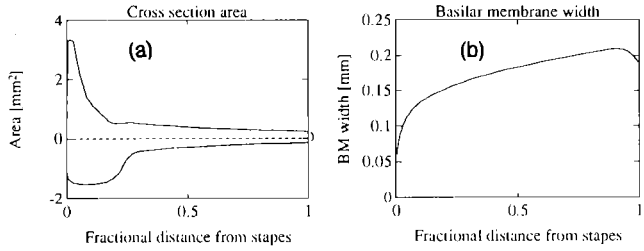

FIG. 1. (a) Cross-section area of the uncoiled guinea-pig cochlea. (b) Width of the basilar membrane of the guinea-pig cochlea (both from Fernández, 1952).

their time derivatives, the motion equation of the BM for the passive cochlea is

$$m(x)\partial_t^2\xi(x,t)+h(x)\partial_t\xi(x,t)+[\partial_x s(x)\partial_x]\partial_t\xi(x,t)$$
$$+k(x)\xi(x,t)=F_S(x)+F_{\mathrm{BM}}(x), \qquad (1)$$

where $x\in[0,1]$ is the *normalized* BM coordinate in the longitudinal direction ($x=0$ and $x=1$ are the abscissas of the stapes and the helicotrema, respectively), t is time, $\xi(x,t)$ is the vertical displacement of the BM, ∂_x is the partial derivative after x, and ∂_t is the partial derivative after t. $F_S(x)$ and $F_{\mathrm{BM}}(x)$ are the external forces acting upon the segment at x due to the fluid pressure differences across the BM, as discussed at the end of this section. Local coefficients $m(x)$, $h(x)$, $s(x)$, and $k(x)$ are discussed in the following term-by-term analysis of Eq. (1).

The *mechanical inertial* term:

$$m(x)\partial_t^2\xi(x,t), \qquad (2)$$

accounting for the local inertial reaction of the organ of Corti, where $m(x)$ is the mass per unit length (kg/m) of the organ of Corti. We assume that $m(x)$ is proportional to the BM width $b(x)$ [Fig. 1(b)] multiplied by the thickness of the organ of Corti [Fig. 2(a)].

The *fluid viscosity* term:

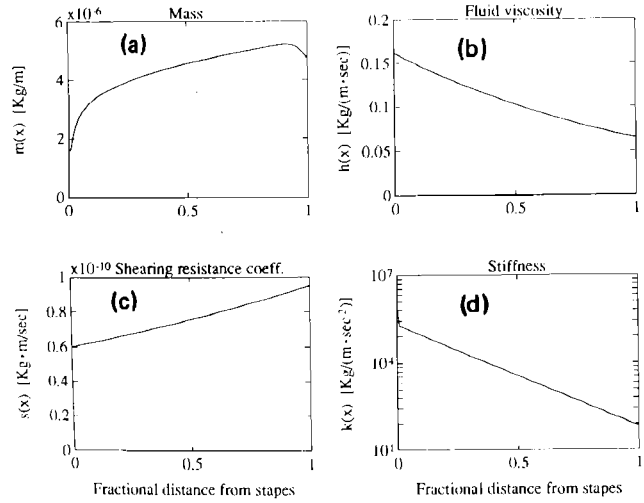

FIG. 2. Relevant physical quantities of the cochlear partition, all defined per unit length: (a) mass $m(x)$; (b) fluid viscosity coefficient $h(x)$; (c) shearing resistance coefficient $s(x)$; and (d) stiffness $k(x)$.

$$h(x)\partial_t\xi(x,t),$$

where coefficient $h(x)$ (kg/m s) accounts for all resistances affecting the absolute vertical motion of the organ of Corti. A simple dimensional computation shows that below 20 dB SPL the Reynolds numbers associated with the motion of the different parts of the cochlear system are smaller than 15 in the cochlear duct and smaller than 0.01 in the narrow cleft (1–5 μm) separating the RL from the TM. Hence, the fluid dynamics is simply affected by viscous forces in laminar regime. As the resistance due to the shearing motion of the fluid within the RL–TM cleft is at least two orders of magnitude larger than all the others (although the motion is contrasted by the elastic reaction of the OHC stereocilia), $h(x)$ can be expressed as

$$h(x)\approx\tau_c[b_c(x)/\epsilon(x)]\sin\theta(x), \qquad (3)$$

where $\tau_c=1.5\times10^{-3}$ kg/m s is the endolymph viscosity (von Békésy, 1960), $b_c(x)$ is the radial width of the cleft, $\epsilon(x)$ the effective cleft height, and $\theta(x)$ the angle formed by the TM and BM rotating planes [as the relative shearing displacement between the RL and the TM is $\xi(x,t)\sin\theta(x)$]. Taking 100 μm for $b_c(0)$, 0.5 μm for the effective $\epsilon(0)$ and $\theta(0)\approx45°$, we estimate $h(0)\approx0.16$ kg/m s. As the width/height ratio of the cleft decreases by about five times from base to apex and $\theta(x)$ by about 1.3 times, we assume $h(x)$ to vary along the cochlea, as shown in Fig. 2(b).

The *shearing resistance* term:

$$[\partial_x s(x)\partial_x]\partial_t\xi(x,t), \qquad (4)$$

where $s(x)=\tau_s S_c(x)$ (kg m/s), τ_s being the average shearing viscosity coefficient of an organ-of-Corti section and $S_c(x)$ the effective area of the section at x. Although experimental values for τ_s are lacking, because of the TM peculiar ultrastructure the resistance due to the shearing motion between adjacent segments of the organ of Corti is likely to be dominated by the internal viscosity of the TM (Hasko and Richardson, 1988). Basing upon dimensional considerations about the fibril structure of the TM matrix, we estimated $\tau_s\approx10\times\tau_c$. Since the TM is moderately tapered, we assume $s(x)$ as represented in Fig. 2(c).

The *fiber stiffness* term:

$$k(x)\xi(x,t),$$

where $k(x)$ (kg/m s^2) is the elastic constant of the cochlear partition with respect to vertical displacement of the BM at x; $k(x)$ receives contributions from the BM fibers, the OHC cytoskeletons (Sec. III), and the limbus–TM–stereocilia–RL system (Sec. IV). It was measured by Gummer *et al.* (1981) in the guinea pig, in the proximity of the site at 1.64 mm from the stapes, using probes with a 25-μm tip diameter. They reported a stiffness plateau upon contacting the BM that usually persisted over the first 2 to 3 μm of static BM displacement, at values 0.34 ± 0.12 N/m. They also reported the plateau stiffness to decrease with increasing distance from the stapes with a space constant of 1.7 ± 0.8 mm and extrapolated a mean plateau value of 1.25 N/m at the stapes. But determining the stiff-

ness by a thin-probe technique yields values underestimated by about a factor of 2 with respect to the effective stiffness of the working cochlea. This is because a point load stretches the membrane differently from a uniform pressure. We have reproduced the frequency map of the guinea-pig cochlea (Greenwood, 1990) by assuming $k(x) = k(0) \times 10^{-3.5x}$ [Fig. 2(d)], where $k(0) \approx 2 \times 10^5$ kg/m s^2 well within the experimental error limits. The exponent 3.5 of $k(x)$ is 1.5 units less than that usually assumed in former theoretical treatments.

The *stapes force* term:

$$F_S(x,t) = -G_S(x)\partial_t^2 \sigma(t), \tag{5}$$

representing the force per unit BM length caused by the stapes motion and transmitted by the fluid to a BM segment at x. Here, $\sigma(t)$ is the stapes displacement at time t. As discussed in Appendix A, the stapes force propagator $G_S(x)$, which has the dimensions of mass per unit length, gives the force per unit length caused by the unit stapes acceleration and acting on the BM site at x.

The *BM force* term:

$$F_{\mathrm{BM}}(x,t) = -\int_0^1 G(x,\bar{x})\partial_t^2 \xi(\bar{x},t)\, d\bar{x}, \tag{6}$$

where $G(x,\bar{x})$ is the Green's function of the fluid pressure field over the BM and has the dimensions of mass per unit area; $G(x,\bar{x})d\bar{x}$ gives the force contribution per unit BM length at site x caused by the unit acceleration of the $d\bar{x}$-long BM segment at $\bar{x}$. So $F_{\mathrm{BM}}(x,t)$ represents the force per unit BM length acting on the BM at x due to the motion of all the BM segments and simultaneously transmitted by the fluid (see Appendix A). This is by far the most important coupling term affecting the dynamics of the cochlear partition.

In order to overcome the deficiencies of previous "box" models, formal expressions and numerical approximations for functions $G_S(x)$ and $G(x,\bar{x})$ are derived in Appendix A for a guinea-pig cochlea with realistic geometry. [Note: In some of the formulas above, the BM width $b(x)$ is implicitly involved. Since the BM is laterally clamped, its vertical displacements are obviously nonuniform across the radial direction. As a result of the peculiar articulation of the organ of Corti segments (see Fig. 5), we shall assume for the effective width $b(x)$ half the geometric width.]

II. RESULTS I: TRAVELING WAVES IN THE PASSIVE COCHLEA

Denoting by $\tilde{a}_\omega$ the Fourier transform of a generic time function $a(t)$ and separating the nonhomogeneous term representing the signal at the stapes from the homogeneous terms depending upon $\xi(x,t)$, the Fourier-transformed version of Eq. (1) is

$$-\omega^2\left(\int_0^1 G(x,\bar{x})\tilde{\xi}_\omega(\bar{x})d\bar{x} + m(x)\tilde{\xi}_\omega(x)\right) + i\omega h(x) + i\omega[\partial_x s(x)\partial_x]\tilde{\xi}_\omega(x) + k(x)\tilde{\xi}_\omega(x) = \omega^2 G_S(x)\tilde{\sigma}(\omega). \tag{7}$$

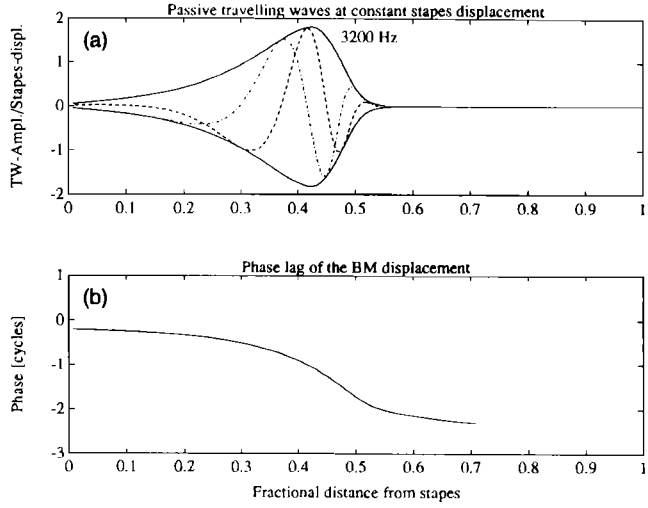

FIG. 3. Traveling wave elicited on the basilar membrane of a passive cochlea by a 3200-Hz sinusoidal vibrations of the stapes (tone), computed as solution of Eq. (9) by numerical inversion of the kernel in Eq. (8) over a 180-points equally spaced grid. (a) Dashed line: real part; dash-dot line: imaginary part; solid line: absolute value. (b) Phase. The abscissa is the normalized basilar membrane coordinate; $x=0$ corresponds to the location of the stapes, $x=1$ to the helicotrema.

This equation can be cast in a compact form by defining the kernel

$$K_\omega(x,\bar{x}) \equiv [k(x) + i\omega h(x) - \omega^2 m(x)]\delta(x-\bar{x}) + i\omega\partial_x[s(x)\partial_x\delta(x-\bar{x})] - \omega^2 G(x,\bar{x}), \tag{8}$$

where $\delta(x-\bar{x})$ is Dirac's delta, which yields the motion equation in the purely integral form:

$$\int_0^1 K_\omega(x,\bar{x})\tilde{\xi}_\omega(\bar{x})d\bar{x} = \omega^2 G_S(x)\tilde{\sigma}(\omega). \tag{9}$$

Equation (9) can be solved for $\tilde{\xi}_\omega(x)$ by numerical inversion of the kernel. Its complex solutions for fixed frequency ω give amplitude and phase of the displacement profiles of the BM. As the phase turns out to be a decreasing monotonic function of x (Fig. 3) these solutions represent traveling waves (TWs).

In a cochlea with uniform section, the TW amplitudes would scale to a good approximation as $k^{1/2}(x)/h(x)$, i.e., about 30 times from base to apex. The TW amplitudes at constant stapes displacement shown in Fig. 4(a) turn out to be comparatively more uniform over a large fraction of the cochlear length. The moderate variability of the TW shapes is a consequence of the peculiar geometry of the cochlear duct and the BM width profile. At constant stapes velocity [Fig. 4(b)] the TW amplitudes scale with frequency in agreement with the pattern shown by Eldredge (1975). Figure 4 also shows that the BM site where a TW reaches its peak is linked to the stimulation frequency by a logarithmic law. Therefore, Eq. (9) accounts for the *tonotopic* organization of the responses of the passive cochlea. Note also that the TW amplitude should not vanish at the helicotrema limit if the BM has a free edge. In our simulations low-frequency TWs undergo a small amount of free-end reflection.

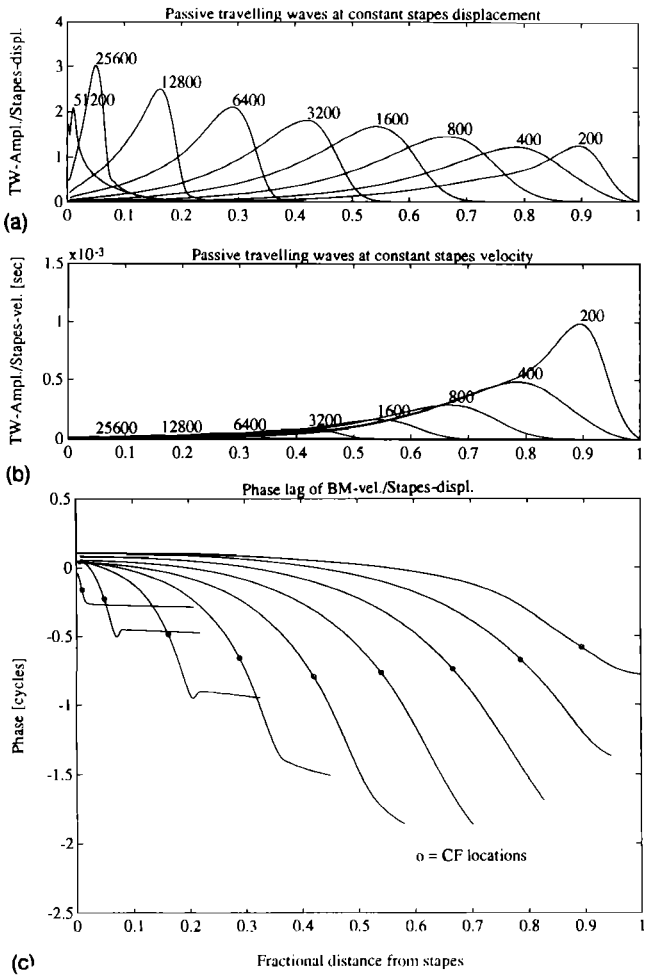

FIG. 4. Traveling waves of the passive cochlea computed as solution of Eq. (9) over a 180-points equally spaced grid for a set of frequencies ordered in a decreasing geometric progression from left to right. (a) Amplitude envelopes at constant stapes displacement; numbers above amplitude peaks indicate tone frequencies. Ordinates are expressed as ratios between basilar membrane displacement and stapes displacement. (b) Amplitude envelopes at constant stapes velocity. Ordinates are expressed as ratios between basilar membrane displacement and stapes velocity. (c) Phases at constant stapes velocity. Phases at constant displacement lag those at constant velocity by $\pi/2$ and are always negative.

III. INTRODUCING OUTER HAIR CELLS

Unlike other cells of the cochlea, OHCs isolated *in vitro* contract if depolarized and elongate if hyperpolarized by amounts so large that the motion can be observed with a light microscope (Brownell *et al.*, 1985). In natural conditions, these motile responses are thought to be elicited by the deflection of the sensory hair bundles (stereocilia) surmounting the OHCs (Hudspeth, 1989). OHCs respond to command pulses under voltage clamp by changing length with a very fast exponential time course, having a characteristic time constant of about 0.6 μs per μm cell length with a mean peak sensitivity of about 20 nm/mV; maximal length changes amount to 4% to 5% of the cell length (Ashmore, 1987). The speed of the motile response ensures that OHCs can operate at acoustic frequencies; length changes have been observed for sinusoidal stimuli at frequencies as high as 30 kHz (Gitter and Zenner, 1988).

Measurements of longitudinal mechanical stiffness of isolated OHCs (Holley and Ashmore, 1988) indicate that the OHC spring-shaped cytoskeletons are stiff enough for the motile responses to transmit forces capable of affecting the mechanics of the organ of Corti. To explain how these forces operate, we shall assume that OHCs are always under tension in normal working conditions. Were the OHC membrane potentials held fixed at their working points, OHC cytoskeletons would simply provide an additive contribution to the mechanical stiffness of the cochlear partition and, in static conditions, the system would be found in a certain equilibrium configuration. Since the additional force provided by the OHCs depends, other things being equal, upon the cell resting length, which in turn depends upon the membrane potential, changing the latter elicits a force tending to change proportionally the equilibrium conditions. Therefore, when the cell electromotility is taken into account, an active force term dependent upon the OHC length changes must be included in the dynamics of the cochlear partition.

IV. THE OUTER HAIR CELL FORCE TERM $U_\omega(x)$

In this section a precise functional form for the force associated with OHC motility will be established by analyzing their transduction properties and triggering mechanism.

A. Outer hair cells and organ of Corti micromechanics

Consider the hypothetical case that the organ of Corti is initially at rest and the OHCs are suddenly *depolarized*. In these conditions, with the organ of Corti subjected only to internal forces, the tunnel of Corti *rotates toward scala tympani* (downward) as the cells contract pulling the RL toward the BM. The rotation is imposed by the rigidity of the framework formed by the RL and the tunnel of Corti itself, which pivots around the base of the inner pillar cells (Fig. 5). Conversely, for the same initial conditions, the tunnel of Corti rotates toward scala media (upward) if the OHCs are hyperpolarized for, in this case, the RL is pushed away from the BM as the OHCs elongate. The configuration of the applied forces is such that the BM tract between the outermost OHC row and the spiral prominence undergoes comparatively small displacements (see inset of Fig. 5).

Consider now the effects of external forces (pressure differences) that induce movements of the BM, for instance *toward scala media*. These cause the deflection of the OHC stereocilia, thought to be firmly attached to the undersurface of the TM (Lim, 1986), in the excitatory direction. This is a consequence of the shearing displacement of the TM with respect to the RL caused by rotation of the tunnel of Corti (Davis, 1958). A transduction current proportional to the deflection of the stereocilia (i.e., to the BM displacement) depolarizes the cells (Russell *et al.*, 1986) and, according to the mechanism illustrated above, an internal force proportional to the BM displacement will then *pull the organ of Corti back*, toward scala tympani. As the opposite happens when the BM moves toward scala tympani, the effect is always such as to oppose its cause. Therefore, in static conditions, i.e., in the zero-frequency

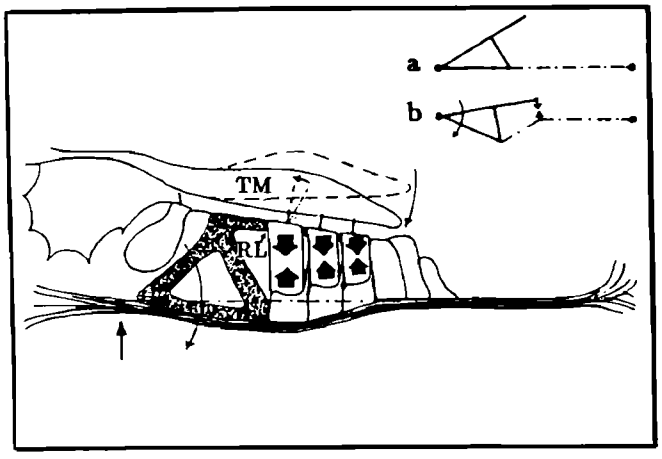

FIG. 5. Contraction of the outer hair cells forces the tunnel of Corti to rotate toward scala tympani (downward). The tunnel pivots approximately about the point indicated by the vertical arrow. The opposite motion is caused by outer hair cells elongation, with the tunnel rotating toward scala media (upward). This is due to the considerable transversal rigidity of the framework formed by the reticular lamina and the pillar cells. But, as the reticular lamina rotates downward (upward), the tectorial membrane shears with respect to it. The stereocilia of the hair cells are deflected in the inhibitory (excitatory) direction, thus forcing the cells to elongate (contract). Since the effect is always such as to oppose its cause, the system admits a state of equilibrium at an intermediate degree of cell contraction. This way, the fibers of the basilar membrane are kept under tension at rest.

limit, the system admits a state of equilibrium at an intermediate degree of OHC contraction. This way, the fibers of the BM are maintained under tension, conceivably at the early stiffness plateau described by Gummer *et al.* (1981) and Olson and Mountain (1991). Owing to the presence of the plateau, the effective stiffness $k(x)$ of the partition *in vivo* (which includes the stiffness of the OHC cytoskeletons) keeps largely independent of cell resting length, thus ensuring the frequency stability of cochlear responses. In the following, the static effect of the OHC force term will be implicitly accounted for by the maintenance of the elastic reaction of the partition at constant plateau values for $k(x)$.

In dynamic conditions the OHC resting length is subjected to variations depending upon the cell membrane potential. Precisely these variations affect the dynamics of the system producing a frequency-dependent *undamping term* $U_\omega(x)$ as a pseudoelastic force term, i.e., a term proportional to the elastic reaction $k(x)\tilde{\xi}_\omega(x)$ of the BM, to be added to the lhs of Eq. (7) with a *positive* sign. In order to establish the frequency dependence of $U_\omega(x)$, the filtering properties of the OHC membrane must be taken into account.

B. Outer hair cells as low-pass filters

Intracellular measurements of the OHC receptor potential recorded *in vivo* in response to tones both in the apical (Dallos, 1985) and the basal end of the cochlea (Cody and Russell, 1987) indicate that the OHC membrane behaves as a simple RC filter with cutoff frequency below 1 kHz. More accurate estimates of the RC cutoffs, derived from experiments on isolated cells, show cutoffs varying from 400 Hz at the base to 15 Hz at the apex (Ashmore and Housley, 1992). As the cell length changes are voltage driven (Ashmore, 1990), the undamping term must be of the type

$$U_\omega(x)=\alpha(x)k(x)l(x)[\tilde{V}_\omega(x)/V_0], \tag{10}$$

where $\alpha(x)$ is an adimensional constant smaller than 1, which accounts for the fraction of $k(x)$ contributed by the OHC cytoskeletons, $l(x)$ is the cell length (in meters), $\tilde{V}_\omega(x)$ the Fourier-transformed receptor potential of the OHCs (in volts), and constant $V_0=2.55$ V is the potential sensitivity of the length change (Ashmore, 1987; Eq. 4, p. 343). $\tilde{V}_\omega(x)$ is in turn related to the Fourier-transformed transducer current $\tilde{I}_\omega(x)$ (in amperes) by the equation

$$\tilde{V}_\omega(x)=\frac{C^{-1}(x)}{\omega_c(x)+i\omega}\tilde{I}_\omega(x), \tag{11}$$

where $C(x)=C_0l(x)$ is the cell capacitance (in farads) and $C_0\approx 0.9$ μF/m; $\omega_c(x)$ is the cutoff frequency of the OHCs at x (in rad/s). In agreement with Housley and Ashmore's data, we put

$$\omega_c(x)=\omega_0\exp(-\gamma x);\quad \omega_0\approx 2\pi\times 400 \text{ rad/s};$$
$$\gamma\approx 3.28. \tag{12}$$

From the little that is known about mammalian OHC transducer currents, in the linear approximation $\tilde{I}_\omega(x)$ is conceivably linked to the stereocilia deflection $\tilde{\zeta}_\omega(x)$ (in meters) by a relationship of the type

$$\tilde{I}_\omega(x)=E_T g_T(x)\tilde{\zeta}_\omega(x), \tag{13}$$

where $E_T\approx 160$ mV is the driving potential and $g_T(x)$ (in siemens/m) the transducer conductance per unit stereocilia deflection (not experimentally determined, to date). The above equation chain yields

$$U_\omega(x)=\frac{n(x)}{\omega_c(x)+i\omega}\tilde{\zeta}_\omega(x), \tag{14}$$

where

$$n(x)=(E_T/C_0V_0)g_T(x)\alpha(x)k(x). \tag{15}$$

Notwithstanding the small value of ω_0 in (12), the maximum frequencies in the guinea pig cochlea are as high as 44 kHz (Greenwood, 1990). This seemingly requires $\tilde{\zeta}_\omega(x)$ to increase appreciably with frequency in order for $U_\omega(x)$ to be effective. To explain how the correct frequency dependence is achieved in the cochlea, the coupling between hair cells and tectorial membrane must be taken into account.

C. Stereocilia stiffness and the tectorial membrane

Basing upon measurements in turns 2, 3, and 4 of the isolated guinea-pig cochlea by Strelioff and Flock (1984), Strelioff *et al.* (1985) estimated that the combined hair-bundle stiffness of an OHC triplet is larger than 1 N/m at the base [comparable to 0.5 N/m for the stiffness of the cochlear partition at the base estimated by Gummer *et al.*

(1981) for a 10-μm BM segment] and decreases exponentially by two to three orders of magnitude from base to apex, giving a range of 10^5–10^3 kg/m s^2 for the stereocilia stiffness per unit length along the cochlea. Hypothesizing that the stiffness of the TM attachment to the limbus is considerably smaller than the cell hair-bundle stiffness, they concluded from these data that each triplet and its overlying TM segment form a resonant mechanical system operating in the audio range and tuned to the local characteristic frequency of the BM. Thus the TM segment would provide the mass and the cell hair bundles elasticity for simple harmonic motion *parallel to the reticular lamina*.

From static measurements in a living cochlea performed by Zwislocki *et al.* (1988), de Boer (1991) concluded that the stiffness of the TM attachment to the limbus is approximately one-seventh of the value measured for the cilia, which confirms the above assumptions. Thus the TM possesses essentially two degrees of freedom: one rotational around the limbus, the other translational in the radial direction. Since the TM is strongly bound to the RL by the stiff OHC stereocilia, the motion of the TM with respect to the RL is a shearing with two independent components. The first one, associated with the rotational degree of freedom, originates from the coordinated rotations of the TM and the tunnel of Corti around their respective pivoting axes, and therefore depends only upon geometric constraints. The second one, associated with the translational degree of freedom, is elicited by the first component in dynamic regimes as a side effect of the TM inertia. The possibility for the TM–OHC system to display a resonant behavior relies upon the second effect.

D. The inertial reaction of the tectorial membrane

Actually, Strelioff *et al.*'s conjecture meets a difficulty because the point-by-point correspondence between the TM–OHC resonances and the BM characteristic frequencies vanishes progressively toward the apical end of the cochlea, where they differ by at least one order of magnitude (as evidenced in Fig. 4 of their paper). Moreover, as stressed by de Boer (1991), it is likely that the stereocilia stiffness in the working cochlea has been underestimated. Considering that the TM oscillations are strongly damped by the TM–RL cleft viscosity, it seems more likely that the transfer-function poles of the oscillating TM segments fall on the frequency complex plane far from the characteristic frequencies of the corresponding BM sites. So the radial motion of the TM relative to the RL is likely to play an important role in enhancing the frequency dependence of the OHC triggering mechanism *without generating tuned secondary resonances*, as explained hereafter.

Consider a harmonic oscillator (not subjected to gravitational forces, for the sake of simplicity) formed by a spring with stiffness k and damping constant h, attached to a point mass m at one end. Let $\xi(t)$ and $\eta(t)$ be the extreme coordinates of the spring, and assume that $\xi(t)$ is a prescribed function of t, while $\eta(t)$ is the coordinate of the point-mass following the system dynamics. Defining the spring elongation as $\zeta(t)=\eta(t)-\xi(t)$, the motion equation is

$$m\ddot{\zeta}(t)+h\dot{\zeta}(t)+k\zeta(t)=-m\ddot{\xi}(t),$$

where the dot notation indicates time derivatives.

The Fourier transform of $\zeta(t)$ is

$$\tilde{\zeta}_\omega=\frac{\omega^2 m}{k+i\omega h-\omega^2 m}\tilde{\xi}_\omega, \tag{16}$$

where Fourier-transformed quantities are represented as usual.

We use this model to simulate the dynamics of the TM–stereocilia–RL system overlying an organ-of-Corti segment interpreting: $\tilde{\xi}_\omega$ as the displacement $\xi_\omega(x)$ of the BM segment at x; $\tilde{\zeta}_\omega$ as the corresponding *radial displacement* $\zeta_\omega(x)$ (m) of the TM with respect to the RL, i.e., the stereocilia deflection; k as the stiffness per unit BM length of the hair bundle triplets $k_s(x)$ (kg/m s^2); h and m, respectively, as the TM–RL cleft resistance $h_s(x)$ (kg/m s) and the mass $m_s(x)$ (kg/m) of the TM at x.

Putting together Eq. (14) and Eq. (16) reinterpreted as described above, the undamping term becomes

$$U_\omega(x)=\frac{\omega^2 n(x)}{[k_s(x)/m_s(x)+i\omega h_s(x)/m_s(x)-\omega^2][\omega_c(x)+i\omega]}\times\tilde{\xi}_\omega(x). \tag{17}$$

Supposing that Strelioff and Flock's data are underestimated by a factor of 2, $k_s(x)$ can be assumed to range from about 4×10^5 kg/m s^2 at the base to about 10^3 kg/m s^2 at the apex. On account of the rather uniform cross section of the TM, the mass term $m_s(x)$ can be assumed to be approximately constant ($m_s\approx3.5\times10^{-6}$ kg/m). The damping factor $h_s(x)$ is essentially equal to $h(x)$ and should vary from about 0.16 kg/m s at the base to about 0.075 kg/m s at the apex. So, with a characteristic frequency $\omega(0)=2.75\times10^5$ rad/s at the base and $\omega(1)=1.25\times10^3$ rad/s at the apex, we find

$$k_s(0)\gg h_s(0)\omega(0);\quad k_s(1)\gg h_s(1)\omega(1)$$

and

$$k_s(0)>m_s\omega^2(0);\quad k_s(1)\gg m_s\omega^2(1).$$

Therefore, in a wide enough frequency range between $\omega_c(0)$ and $[k_s(0)/m_s]^{1/2}$, the undamping term $U_\omega(x)$ can be approximated by

$$U_\omega(x)\approx-i\omega\frac{n(x)m_s}{k_s(x)}\tilde{\xi}_\omega(x). \tag{18}$$

This relationship indicates that, owing to the large values of the stereocilia stiffness $k_s(x)$, the key factor in enhancing the frequency dependence of the OHCs triggering mechanism is the inertial reaction of the TM.

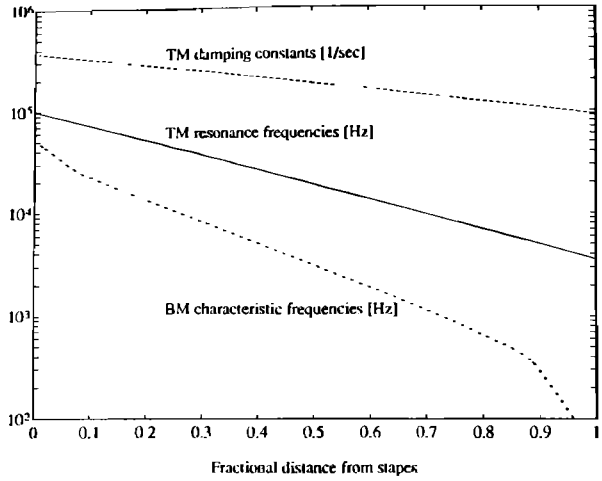

FIG. 6. Resonance frequencies (solid line) and damping coefficient (dashed line) of the tectorial membrane radial motion, compared to the characteristic frequencies of the active cochlea (dash-dot line).

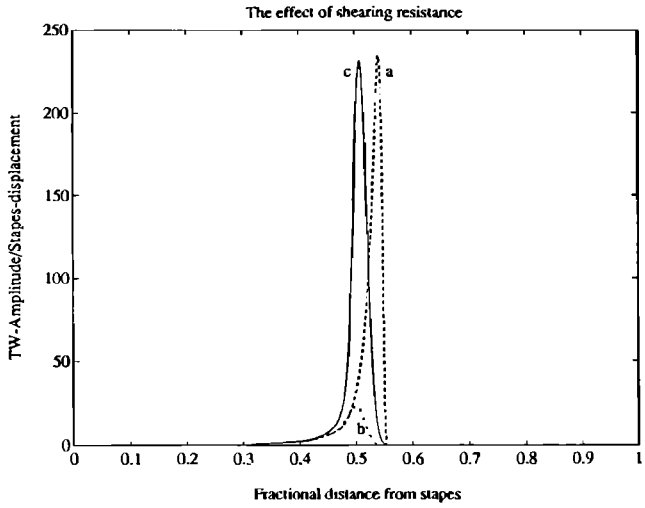

FIG. 7. By the effect of the shearing resistance $s(x)$ the traveling wave peak is smoothed and strongly depressed. To restore the peak size, the outer hair cell activity parameter λ needs to be somewhat increased. (a) Dashed line: $\lambda=1.1$, $s(x)=0$; (b) dash-dot line: $\lambda=1.1$, $s(x)\approx 10^{-10}$ kg m/s; (c) solid line: $\lambda=1.34$, $s(x)\approx 10^{-10}$ kg m/s. Tone frequency is the same as in Fig. 3. Notice that in (a) damping is not completely compensated despite λ is greater than 1 because of the small contribution to the overall partition damping from the tectorial membrane.

V. ACTIVE COCHLEAR DYNAMICS

The velocity dependence of the viscous forces inherent in the cochlear partition can be compensated in an optimal way if the forces applied by OHCs are in phase with and proportional to the BM velocity. For frequencies that are neither too low nor too high, the approximation in Eq. (18) holds. Therefore, term $i\omega h(x)\tilde{\xi}_\omega(x)$ in Eq. (7), describing the fluid viscosity of the partition, can be almost uniformly canceled over the whole cochlear length, provided

$$h'(x)\equiv n(x)m_s/k_s(x)\approx h(x). \tag{19}$$

The cancellation, and therefore the undamping effect of $U_\omega(x)$, will be only partial both at very low and very high frequencies where the approximation in (18) breaks down. Of course, the shearing resistance term cannot be canceled by $U_\omega(x)$, but its damping effect can be contrasted if $h'(x)$ exceeds uniformly $h(x)$ by a small amount.

Recalling the expression of $n(x)$ in (15), it is readily appreciated that, for Eq. (19) to hold, product $\alpha(x)g_T(x)$ must scale precisely as $h(x)k_s(x)/k(x)$, which amounts to about 23 times from base to apex. Although currently available data are insufficient to establish the scaling properties of $g_T(x)$ and $\alpha(x)$, such figure does not seem to exceed physiological limits. Assuming the validity of Eq. (19), the OHC's undamping term becomes

$$U_\omega(x) = \frac{\omega^2 h'(x)}{[1+i\omega\gamma_s(x)/\omega_s^2(x)-\omega^2/\omega_s^2(x)][\omega_c(x)+i\omega]} \times\tilde{\xi}_\omega(x), \tag{20}$$

where resonance frequencies $\omega_s(x)=[k_s(x)/m_s]^{1/2}$ and damping coefficient $\gamma_s(x)=h(x)/m_s$ are shown in Fig. 6. By including this term into the kernel of the passive cochlea, the equation for the active cochlea can be put in the form

$$\int_0^1 H_\omega(x,\bar{x})\tilde{\xi}_\omega(\bar{x})d\bar{x}=\omega^2 G_S(x)\tilde{\sigma}(\omega), \tag{21}$$

where

$$H_\omega(x,\bar{x})=K_\omega(x,\bar{x})+\delta(x-\bar{x})U_\omega(x).$$

VI. RESULTS II: TRAVELING WAVES IN THE ACTIVE COCHLEA

Numerical solutions of Eq. (21), characterized by the rise of marked peaks, were obtained as in the passive case by inversion of the integral kernel with $h'(x)=\lambda h(x)$ in Eq. (20), where $\lambda\in[0,1+c]$ is a parameter introduced in order to control the amount of residual damping (c is a small positive number). It represents the degree of efficiency of the OHC motile responses for, the closer λ to 1, the better damping due to the fluid viscosity is canceled. A certain overcompensation, represented by c, is needed for contrasting also the resistance due to the shearing motion between adjacent segments of the organ of Corti, as well as the TM impedance. As mentioned in the previous section, the shearing resistance term cannot be canceled by this procedure. But, being small, it is effective only for vanishing wavelengths of the TW amplitudes, i.e., on the falling edge of the TW. As shown in Fig. 7, it produces a marked smoothing of TW peaks. Since damping is compensated without violating the stability conditions of the system, the structural stability of the cochlear function is guaranteed.

A set of TW with inclusion of OHCs, to be compared to those in Fig. 4, are shown in Fig. 8. Isoamplitude tuning curves, as defined in Sellick *et al.* (1983), and respective phases are compared to experimental data in Figs. 9 and

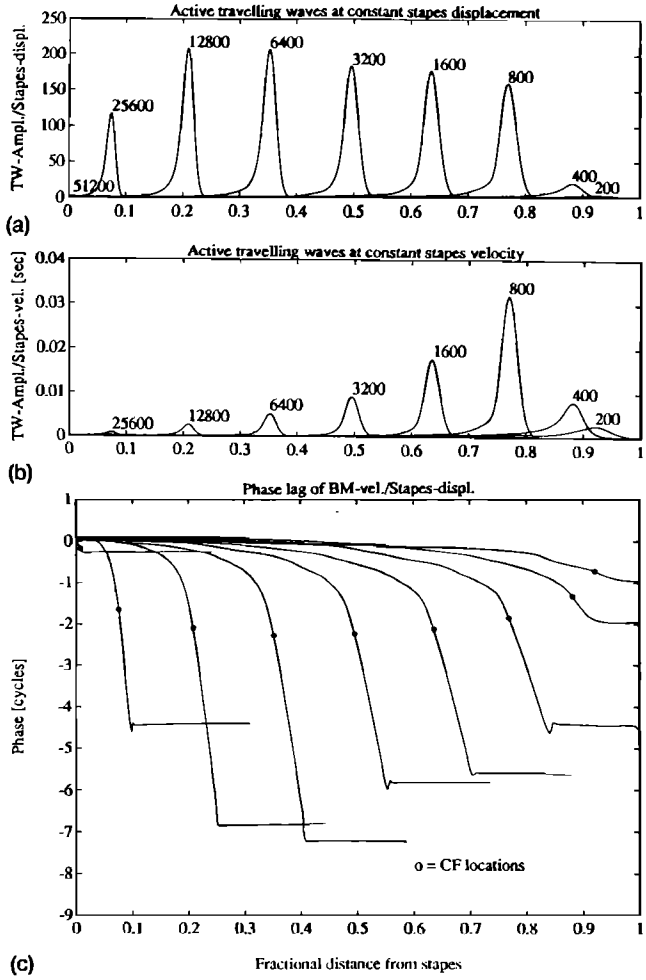

FIG. 8. Traveling waves elicited on the active basilar membrane by sinusoidal vibrations of the stapes, computed as solutions of Eq. (21) for $\lambda=1.35$. All others parameters have the same values used in Fig. 4. (a) Amplitude envelopes at constant stapes displacement. Numbers above wave peaks indicate tone frequencies. Ordinates are expressed as ratios between basilar membrane displacement and stapes displacement. (b) Amplitude envelopes at constant stapes velocity. Ordinates are expressed as ratios between basilar membrane displacement and stapes velocity. (c) Phases at constant stapes velocity. The abscissa represents the normalized basilar membrane coordinate. Quantization errors associated with the peaked character of these solutions were overcome by introducing a variably spaced grid for the matrix representation of the integral kernel, which increased the density of grid points in the peak region by a factor up to 60. The overall number of points was maintained about 200, which kept the C.P.U. time within reasonable limits (approximately 4 min per traveling wave on a 386 P.C.). The shape of the maximum-amplitude profile is sensitive to the tectorial membrane mass $m_s(x)$ and the exponent of the stereocilia stiffness $k_s(x)$ (see Sec. IV) although the local resonances of the tectorial membrane are severely damped by the viscosity in the cleft separating the membrane from the reticular lamina, and lie far from the corresponding characteristic frequencies of the basilar membrane.

10, where the effect of decreasing the efficiency of OHC motility was simulated by decreasing λ from 1.34 (active case) to zero (passive case).

VII. DISCUSSION

As is well known, the main problem concerning the effectiveness of outer hair cells in enhancing to an extraordinary level the frequency selectivity of the cochlea lies in

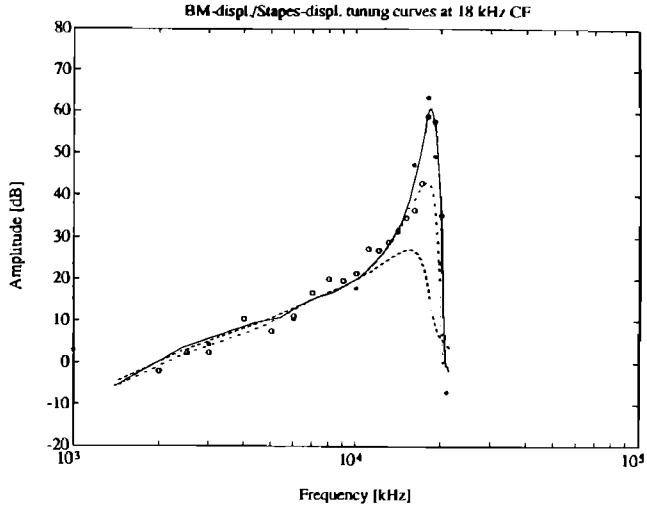

FIG. 9. Isovelocity tuning curves for a few values of the damping-control parameter λ: $\lambda=1.34$ (solid line); $\lambda=1.25$ (dash-dot line); $\lambda=0$ (dashed line). Tuning curves were generated by solving Eq. (21) for a number of different frequencies, i.e., producing a family of TWs, and selecting amplitudes and phases at a fixed BM site x for each frequency value. Stars (*) and opens symbols (O) data from and Sellick *et al.* (1983).

that these cells behave as mechanical effectors with low-pass filter characteristics. The cutoff frequencies of the outer hair cell membrane are below 400 Hz. On the other hand, cutoffs much higher than those observed would be incompatible with the constraints imposed by the physics of biological systems. Thus, in the absence of suitable compensatory effects, the voltage-controlled motile responses of outer hair cells would be negligible for frequencies above approximately 1 kHz.

We envisaged the cunning solution by which nature has been able to circumvent this difficulty in the inertial reaction of the tectorial membrane that makes the triggering mechanism of outer hair cells increase as the square of frequency over a wide frequency range provided the reso-

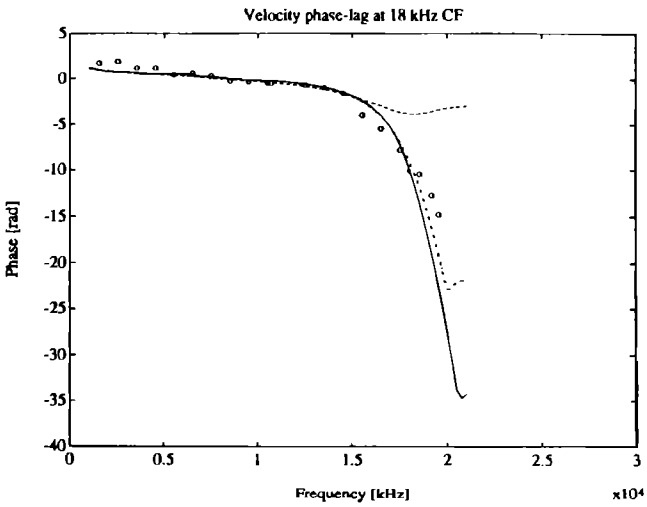

FIG. 10. Velocity phase lag of the tuning curves shown in Fig. 9 for the same values of the damping-control parameter. Open symbols (O): data from Sellick *et al.* (1983).

nances of the tectorial membrane are smooth and fall appreciably beyond the corresponding characteristic frequencies. In order for this mechanism to work properly, large values for the stiffness of the cell stereocilia are required. Experimental data are consistent with this conclusion.

Our thesis is that, thanks to the triggering enhancement due to the tectorial membrane inertia, the outer hair cells are capable of compensating the dissipative losses due to the inherent viscosity of the cochlear partition. This imposes precise constraints on the size of the receptor currents. We know from experiments that the efficiency of the cochlear amplifier is maximal for near-threshold sound-pressure levels. At 20 dB SPL the basilar membrane displacements are about 0.6 nm, at least for characteristic frequencies in the interval from 8 to 18 kHz. The damping force per unit length of the cochlear partition at these frequencies is as large as the elastic reaction of the basilar membrane (Fig. 2). Consequently, the outer hair-cell length changes must be as large as the basilar membrane displacements in order to produce undamping forces of the right magnitude. Since the cell motile sensitivity is approximately 20 nm/mV (Ashmore, 1987) and the transducer current is linked to the receptor potential by the capacitive impedance of the cell [Eq. (11)], the current must be as large as 360 pA when the stereocilia are deflected by less then 1 nm. The largest values reported by Kros *et al.* (1992) *in vitro* are about 700 pA, but unfortunately the relationship between current and cilia deflection has not been measured yet.

The predicted frequency dependence of the transducer current may appear in contrast with the intracellular recordings of outer hair cells response to tones *in vivo* (Cody and Russell, 1987), which showed negligible receptor potentials (hence transducer currents) at high frequencies for near-threshold stimuli. But it should be considered that placing a microelectrode severely limits the local oscillations of the organ of Corti since the stiffness of a microelectrode is orders of magnitude larger than that of the basilar membrane. Thus the dependence of the transducer current upon the acceleration of the tectorial membrane is suppressed and the current turns out to be proportional to the local fluid pressure (that is, ultimately, to the local displacement of the tectorial membrane).

In previous approaches (Allen, 1977; Neely and Kim, 1986; Kolston, 1988; Kolston *et al.*, 1990), the cochlea was treated as a "box" with a constant rectangular cross section and simple transmission-line partial differential equations were derived. Unfortunately, the radius of the cross sections of the guinea-pig cochlear duct increases abruptly (like that of a trumpet) toward the base, whereas the BM width decreases markedly, so that the ratio of the two can be as large as 20, or even more, in the high-frequency region of the cochlea (Fernández, 1952). The trumpet stem spans two-thirds of the entire cochlear length. So these approximations are reasonable only in the apical fraction, for which reliable experimental data are lacking. Moreover, active transmission-line models (e.g., Zwicker, 1986; Neely and Kim, 1986) are characterized by *ad hoc* frequency-dependent negative-damping terms that, although capable of enhancing the magnitude of the response, tend to distort the phase. Whereas, as found by Ruggero and Rich (1991), the phase is a monotonically decreasing function of frequency, with "passive" phases almost superimposed on the "active" ones up to the characteristic frequency of the site.

In Appendix A we have computed the Green's function for a realistic profile of the guinea-pig cochlear duct. The Green's function formalism leads naturally to an integral-equation approach which we prefer as, besides producing phase and amplitude behaviors in agreement with experimental data, it accounts more accurately for the effect of the fluid boundary on the dynamics of the cochlear partition. In fact, replacing an integral equation for cochlear motion with a differential equation plus suitable boundary conditions, as done most clearly by Allen (1977) and by Steele and Taber (1979), yields roughly approximated solutions in the small wavelength domain. It is legitimate only if smooth enough solutions are expected and the cochlear duct boundaries have simple geometry. The double differentiation used to convert cochlear integral equations into equivalent partial differential equations works correctly only if: (1) The logarithmic singularity of the Green's function can be treated as a Dirac's delta, i.e., if the factor in the integrand is a smooth function; (2) the long-range tracts of the Green's function are approximately linear. In Allen's box model (Allen, 1977) the Green's function, computed with the image-charge method, is nearly constant on the left side of the singularity and decreases linearly on the right side as a consequence of the simplified geometry. So both these tracts are removed by double differentiation. But, if the longitudinal variability of geometrical parameters is considered (cochlear duct shape and size, basilar membrane width, etc.), the long-range action of the Green's function [Fig. 13(b)] cannot be canceled by multiple differentiation and the full integral-equation technique must be applied. More critically, highly undamped traveling waves undergo extreme space-oscillatory shrinking in the proximity of their peaks. Since extremely peaked solutions are expected for the active cochlea, the extended structure of the Green's function singularity (see Appendix A) must be considered and not simply approximated by a Dirac's delta. Finally, solving integral equations by a matrix-inversion technique is simpler and more direct than trying to build up and integrate high-order differential equations, as these also necessitate correctly stating boundary conditions.

A limitation of the present approach is the obvious impossibility to account for the interesting repertoire of nonlinear phenomena which are known to affect the mechanics of the cochlea at medium–large sound intensities (see, for instance, Johnstone *et al.*, 1986).

ACKNOWLEDGMENTS

We wish to express our gratitude to Jonathan Ashmore, Paul Kolston, and two anonymous reviewers for their criticism and advice. We are also grateful to Matthew Holley for his comments on the complex anatomy of the organ of Corti.

APPENDIX A: THE STAPES AND BASILAR MEMBRANE FORCE TERMS

The force terms $F_S(x,t)$ and $F_{BM}(x,t)$, introduced in Sec. I, are proportional to the pressure difference across the BM. They summarize the actions, simultaneously transmitted by the fluid, produced respectively by the stapes and the whole BM on the BM segment at x. Let $\mathbf{r}$ be the position vector representing a point within the fluid. In the limit of small fluid-boundary displacements and velocities, the pressure field $p(\mathbf{r})$ of an incompressible fluid and the local fluid acceleration $\mathbf{a}(\mathbf{r},t)=\partial_t \mathbf{v}(\mathbf{r},t)$, where $\mathbf{v}(\mathbf{r},t)$ is the velocity field and ∂_t indicates partial time derivative, are linked by Euler equation

$$\nabla p(\mathbf{r},t)+\rho \mathbf{a}(\mathbf{r},t)=0, \tag{A1}$$

where ρ is fluid density and ∇ is the gradient operator after $\mathbf{r}$. Under the assumed conditions the velocity field is irrotational. Moreover, its divergence is zero because of fluid incompressibility. Therefore, we can put $\mathbf{v}(\mathbf{r},t)=\nabla\phi(\mathbf{r},t)$, where $\phi(\mathbf{r},t)$ is a scalar field, called *velocity potential* (see, for example, Tritton, 1977). Then, Eq. (A1) can be integrated all over the fluid yielding

$$p(\mathbf{r},t)+\rho\partial_t\phi(\mathbf{r},t)=\text{const}; \tag{A2}$$

$\phi(\mathbf{r},t)$ satisfies Laplace equation $\nabla^2\phi(\mathbf{r},t)=0$ with boundary conditions $\nabla\phi(\mathbf{r}_b,t)=\mathbf{v}(\mathbf{r}_b,t)$, where $\mathbf{v}(\mathbf{r}_b,t)$ is the velocity of the cochlear fluid at the boundary position vector $\mathbf{r}_b$ [the component of $\mathbf{v}(\mathbf{r}_b,t)$ orthogonal to the fluid boundary vanishes everywhere except at the surface of stapes and BM].

Let us indicate respectively by $p_+(x,t)$ and $p_-(x,t)$ the fluid pressure just above and below the BM segment at point x and time t, and with $\phi_+(x,t)$ and $\phi_-(x,t)$ the corresponding velocity potentials. Then, Eq. (A2) gives the following expression for the total force per unit length (N/m) caused by the motion of the cochlear boundary

$$\begin{aligned} F_S(x,t)+F_{BM}(x,t)&=b(x)[p_-(x,t)-p_+(x,t)] \\ &=\rho b(x)\partial_t[\phi_+(x,t)-\phi_-(x,t)], \end{aligned} \tag{A3}$$

where $b(x)$ is the effective BM width (see note in the Introduction). So, provided the velocity potentials above and below the BM at x are known at any time t, the hydrodynamic effects of the cochlear motion are completely determined by the differences $\phi_+-\phi_-$. These can be formally obtained as follows.

As long as the vibrating fluid boundaries do not change their average position, the isopotential surfaces of ϕ do not depend on t. Let us indicate by $S_+(x)$ and $S_-(x)$ the isopotential surfaces (as well as their areas) of the potentials $\phi^s_\pm(x,t)$ generated by the motion of the stapes alone and intersecting the BM at x respectively from above and below. Since the divergence of $\mathbf{v}(\mathbf{r},t)$ is zero, its instantaneous space-averaged values $\bar v_+(x,t)$ and $\bar v_-(x,t)$, respectively, orthogonal to $S_+(x)$ and $S_-(x)$, satisfy the constant-flux condition $\bar v_\pm(x,t)S_\pm(x)=\bar v_\pm(x',t)S_\pm(x')$ for different x, x'. Let $l_\pm(x)$ be the curvilinear coordinate along the medial line crossing the family of surfaces $S_\pm(x)$ from base ($x=0$) to apex ($x=1$) [Fig. A1(a)]. Then

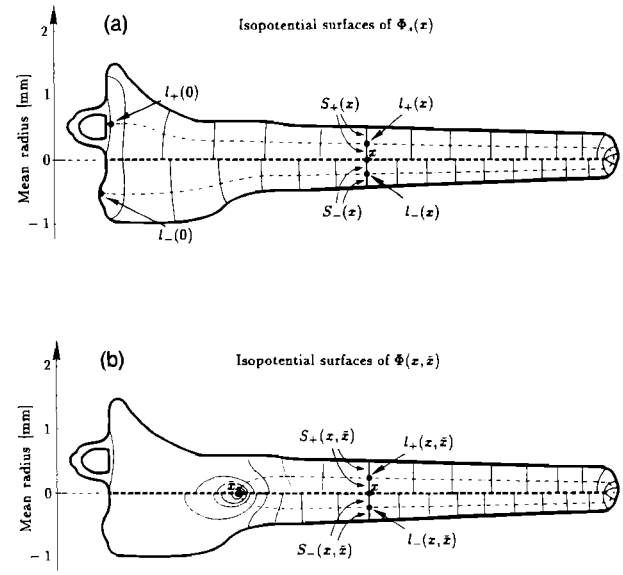

FIG. A1. (a) Isopotential surfaces $S_\pm(x)$ (thin solid lines) and related medial lines $l_\pm(x)$ (dash-dot symbols) for the velocity potential generated by the motion of the stapes. (b) Isopotential surfaces $S_\pm(x,\bar x)$ and related medial lines $l_\pm(x,\bar x)$ for the potential generated by the motion of a basilar membrane segment at x. The outer contour of the cochlea is shown as a thick solid line. The basilar membrane is represented as a horizontal dashed line.

$$\begin{aligned} \phi^s_\pm(x_2,t)-\phi^s_\pm(x_1,t)&=\int_{x=x_1}^{x=x_2}\bar v_\pm(x,t)\,dl_\pm(x) \\ &=S_\pm(x_1)\bar v_\pm(x_1,t)\int_{x=x_1}^{x=x_2}\frac{dl_\pm(x)}{S_\pm(x)}. \end{aligned}$$

To determine $F_S(x,t)$ we integrate along $l_\pm(x)$ from $x=0$ to x, which yields

$$\phi^s_+(x,t)=S\partial_t\sigma(t)\int_{x'=0}^{x'=x}\frac{dl_+(x')}{S_+(x')}+C,$$

$$\phi^s_-(x,t)$$

$$=S\partial_t\sigma(t)\left(\int_{x'=0}^{x'=1}\frac{dl_+(x')}{S_+(x')}+\int_{x'=1}^{x'=x}\frac{dl_-(x')}{S_-(x')}\right)+C,$$

where S and $\sigma(t)$ are surface and displacement of the stapes, respectively, and C is an integration constant. Defining

$$G_S(x)\equiv\rho S b(x)\int_{x'=x}^{x'=1}\left(\frac{dl_+(x')}{S_+(x')}+\frac{dl_-(x')}{S_-(x')}\right), \tag{A4}$$

we obtain an explicit expression for Eq. (5).

In a similar way we can formally determine the contribution to the velocity potential from the acceleration $\partial_t^2\xi(\bar x,t)$ of the $d\bar x$-long BM segment at $\bar x$ alone. Let $S_\pm(x,\bar x)$ be the families of equipotential surfaces of the potential generated by the motion of this segment and $l_\pm(x,\bar x)$ their medial curvilinear coordinates [Fig. A1(b)]. These surface families differ significantly among themselves, depending on coordinate $\bar x$. Integrating the averaged velocity field $\bar v_\pm(x,\bar x,t)$ generated by the $\bar x$ segment along

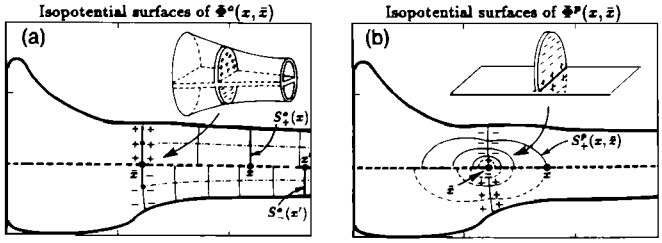

FIG. A2. (a) Isopotential surfaces $S^0_+(x)$ and $S^0_-(x')$ for the long-range parts $\phi^0_\pm(x,\bar{x})$ of the velocity potentials $\phi_\pm(x,\bar{x})$; inset: semidisk-shaped source distributions generating the isopotential surfaces; (b) isopotential surfaces $S^p_+(x,\bar{x})$ for the short-range part $\phi^p_+(x,\bar{x})\equiv\phi_+(x,\bar{x})-\phi^0_+(x,\bar{x})$ of the velocity potential in the upper cochlea semispace; inset: comprehensive source distributions generating the singularity contribution and its BM-mirrored image.

$l_\pm(x,\bar{x})$, the segment contribution to $F_{\rm BM}(x,t)$ is found to be proportional to $\partial_t^2\xi(\bar{x},t)\,d\bar{x}$ multiplied by

$$G(x,\bar{x}) \equiv \rho b(x)b(\bar{x})\int_{x'=x}^{x'=1}\left(\frac{dl_+(x',\bar{x})}{S_+(x',\bar{x})}+\frac{dl_-(x',\bar{x})}{S_-(x',\bar{x})}\right). \quad \text{(A5)}$$

This provides an explicit expression for Eq. (6).

Expressions (A4) and (A5) indicate that the stapes propagator $G_S(x)$ and cochlea Green's function $G(x,\bar{x})$ can be computed by determining the shape of the isopotential surfaces of the velocity potential at any point within the fluid.

Exact expressions for $G(x,\bar{x})$ could be derived for fluid boundaries with simple symmetry properties (see Allen, 1977). But in the general case the exact shape of the isopotential surfaces is not easily determined in the neighborhood of $x=\bar{x}$, where $G(x,\bar{x})$ becomes singular. Therefore, the procedure illustrated above can be used only to compute $G(x,\bar{x})$ away from the singularity region, outside of which $S_\pm(x',\bar{x})$ are well approximated by the cochlear duct sections $S^0_\pm(x')$ {which of course do not depend upon $\bar{x}$ [Fig. A2(a)]}.

The general-case problem can be tackled by taking advantage of the Green's function linearity, separating it into its long- and short-range parts. We define the long-range part $G_0(x,\bar{x})$ as in (A5), with substitutions

$$S_\pm(x',\bar{x})\to S^0_\pm(x'), \quad dl_\pm(x',\bar{x})\to dx'.$$

This is tantamount to replacing the segment-shaped velocity-field sources at x (which have opposite signs and lie on the opposite sides of the BM) with a suitable pair of semidisk-shaped source distributions opposite in sign and occupying the upper and lower semisections of the cochlear duct at x, the boundary conditions for the velocity field being unchanged [Fig. A2(a)]. The integral for $G_0(x,\bar{x})$, which depends only upon the geometry of cochlear duct and BM, can be easily computed. It turns out to be constant for $\bar{x}<x$ and to decrease progressively to a small value for $\bar{x}\to 1$. In our simulations, numerical values for $G_0(x,\bar{x})$ were obtained using data from Fernández (1952) for $S^0_\pm(x')$ and $b(x)$ (Fig. 1).

The short-range part of the Green's function

$$G_p(x,\bar{x})\equiv G(x,\bar{x})-G_0(x,\bar{x})$$

can be computed from the differences of the short-range parts of the velocity potentials

$$\phi^p_\pm(x,\bar{x})\equiv\phi_\pm(x,\bar{x})-\phi^0_\pm(x,\bar{x}),$$

which represent the singularity contributions to $\phi_\pm(x,\bar{x})$ generated by the BM segment at x (in order to simplify the notation, here and in the following we do not indicate explicitly the dependence of the velocity potentials upon time, leaving it understood). Here, $\phi^p_\pm(x,\bar{x})$ are equivalent to the velocity potential generated by the aforementioned segment-shaped sources, above and below the BM, together with the semidisk-shaped sources taken with opposite sign [Fig. A2(b)]. Also for this source distribution the boundary conditions are unchanged. But, owing to the multipolar character of the distribution, the range of influence of $\phi^p_\pm(x,\bar{x})$ over the BM is confined to a distance comparable to the local cochlear duct radius. In these conditions the effects of the cochlear walls on the BM can be safely neglected. Therefore, the only *effective* boundary condition to be taken into account is the source mirroring due to the BM [see inset of Fig. A2(b)].

Following this approach we determined analytically approximated expressions for short-range term $G_p(x,\bar{x})$, a sampled representation of which is given by the set of peaked curves in Fig. A3(a). Green's function $G(x,\bar{x})$, sampled at various values of x, is shown in Fig. A3(b), whereas $G_S(x)$ is shown in Fig. A3(c). We assumed that $G_S(x)$ is well approximated by $G(0,x)$ except for a proportionality constant and the singularity at $x=0$. This is tantamount to assuming that the velocity field generated by the stapes is similar to that generated by the BM segment nearest to the stapes [programs for the evaluations of $G(x,\bar{x})$ are available on request]. We verified that applying this method to a rectangular-section duct produces negligible differences with respect to Allen's (1977) result. We are confident that it produces acceptable approximations also for the general case.

Finally, notice that

$$\bar{G}\equiv\int_0^1\int_0^1 G(x,\bar{x})\,dx\,d\bar{x},$$

which represents the hydrodynamic mass loading the BM when the membrane is rigidly displaced all along its length, is such that

$$\bar{G}/\bar{M}\approx 1500, \quad \text{with } \bar{M}\equiv\int_0^1 m(x)dx, \quad \text{(A6)}$$

$\bar{M}$ being the total mass of the organ of Corti. The large value of this ratio, which is hydrodynamic in origin, indicates that it would be wrong to refer the characteristic frequencies of the BM to $[k(x)/m(x)]^{1/2}$ as for the harmonic oscillators. In Allen's box model (Allen, 1977) the analogous ratio is well approximated by $L^2/(3H_cH_p)\approx 1140$, where L is the length of the uncoiled cochlea (18.5 mm), H_c the height of the scalae (1 mm) and H_p the height of the cochlear partition (0.1 mm).

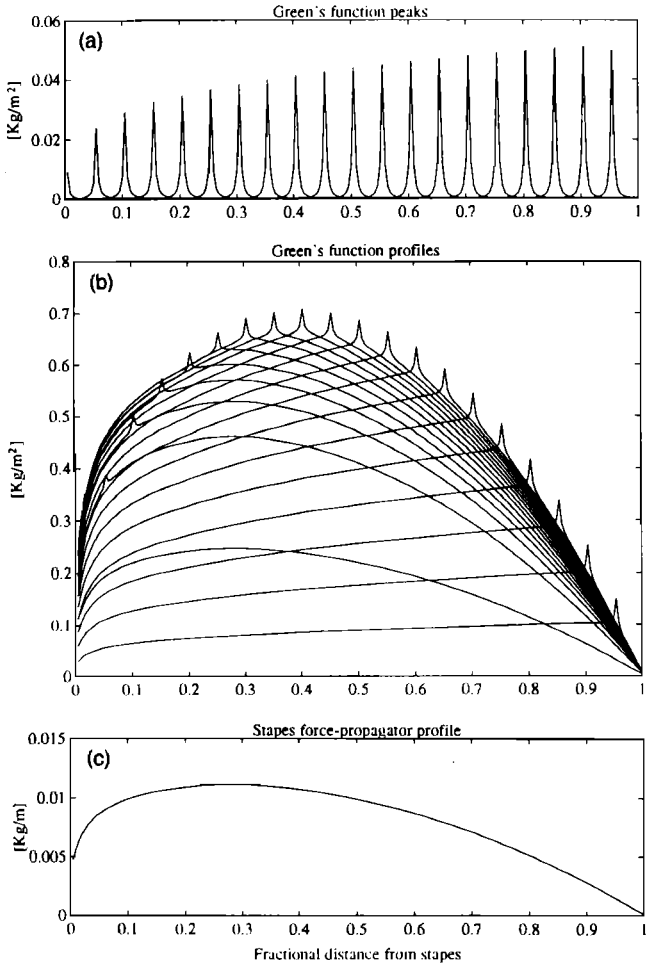

FIG. A3. (a) Samples of the singular part $G_p(x,\bar{x})$ of the Green's function for several x values as functions of $\bar{x}$. (b) Analogous samples for the whole Green's function $G(x,\bar{x})$ [Eq. (A5)]. Notice the different scale used to plot peaks in (a). (c) Stapes propagator $G_S(x)$ [Eq. (A4)].

APPENDIX B: LONGITUDINAL ELASTIC COUPLING IS NEGLIGIBLE

Longitudinal elastic coupling between adjacent segments of the organ of Corti depends critically on the structure of the RL and the TM. The joined upper portions of the pillar cells form an arch-shaped prominence extending to the cuticular plate of the first series of OHCs. This arch possesses peripheral thickenings which, joined together and to the thickenings contouring the OHC cuticular plates and the ends of Deiter's cell phalanges, are closely tiled to form the RL (Iurato, 1961; Voldřich, 1983). This is paved according to a hexagonal symmetry. Because of its peculiar morphology, characterized by a systematic thickening of the cell junctions in the radial direction and by the deformable contours of the phalangeal processes in the longitudinal direction, the RL is expected to be rather stiff under bending around longitudinal axes, but somewhat compliant under longitudinal stretching or compression.

The TM is a gelatinous mass attached to the modiolar side of the cochlear duct and to the organ of Corti (Steel, 1986). Within the TM, a prominent system of radial fibers (type A) are embedded in the matrix of type B protofibrils, which seem to constitute the TM ground substance (Hasko and Richardson, 1988). Type A fibers are almost certainly type II collagen fibrils, whereas type B fibers, which are extensively cross-linked and organized in sheets, are formed by noncollageneous, glycosilated polypetides. None of these fibers appear under tension, so that the TM can be regarded as incapable of contrasting longitudinal deformations, its main function being that of transmitting mechanical excitation to the stereocilia of the hair cells in the radial direction.

These conclusions can be put in a more quantitative form as follows. The dynamics of an elastic sheet vary depending on whether it is thick or thin and under tension or not. If it is thick, the square-Laplacian term, expressing the elastic reaction to local flexions, cannot be ignored. If it is under transverse tension, no matter how thin the sheet, the Laplacian term (expressing the elastic reaction to shearing displacements) cannot be ignored. If it is thin and not under transverse tension, the main space-derivative term is proportional to the squared gradient of the vertical-displacement times its Laplacian, i.e. (in our context) $[\partial_x \tilde{\xi}_\omega(x)]^2 \partial_x^2 \tilde{\xi}_\omega(x)$, and is therefore negligible as far as small amplitudes are involved.

Because of the segmental structure of the organ of Corti and since the applied forces are vertical, torques around radial axes are negligible and the elastic longitudinal coupling depends mainly on the small elastic reaction of the RL and the TM to shearing displacements between adjacent segments. In other words, as far as longitudinal coupling is concerned, the organ of Corti behaves like a free viscoelastic strip. Since under normal sound excitations $|\partial_x \tilde{\xi}_\omega(x)|$ is less than 10^{-2}, longitudinal elastic coupling is negligible in the small-amplitude approximation.

Allen, J. B. (**1977**). "Two-dimensional cochlear fluid model: New results," J. Acoust. Soc. Am. **61**, 110–119.

Ashmore, J. F. (**1987**). "A fast motile response in guinea-pig outer hair cells: the cellular basis of the cochlear amplifier," J. Physiol. **388**, 323–347.

Ashmore, J. F. (**1990**). "Forward and reverse transduction in the mammalian cochlea," Neurosci. Res. Suppl. **12**, S39–S50.

Ashmore, J. F., and Housley, G. D. (**1992**). "Ionic currents of outer hair cells isolated from the guinea-pig cochlea," J. Physiol. **448**, 73–98.

Békésy, G. von (**1960**). *Experiments in Hearing* (McGraw-Hill, New York).

Brownell, W. E., Bader, C. R., Bertrand, D., and de Ripaubierre, Y. (**1985**). "Evoked mechanical responses of isolated cochlear hair cells," Science **227**, 194–196.

Cody, A. R., and Russell, I. J. (**1987**). "The response of hair cells in the basal turn of the guinea pig cochlea to tones," J. Physiol. **383**, 551–569.

Dallos, P. (**1985**). "Response characteristics of mammalian cochlear hair cells," J. Neurosci. **5**, 1591–1603.

Davis, H. (**1958**). "Transmission and transduction in the cochlea," Laryngoscope **68**, 359–382.

Davis, H. (**1983**). "An active process in cochlear mechanics," Hear. Res. **9**, 79–90.

de Boer, E. (**1980**). "Auditory physics. Physical principles in hearing theory. I," Phys. Rep. **62**, 87–174.

de Boer, E. (**1983**). "No sharpening? A challenge for cochlear mechanics," J. Acoust. Soc. Am. **73**, 567–573.

de Boer, E. (**1984**). "Auditory physics. Physical principles in hearing theory. II," Phys. Rep. **105**, 141–226.

de Boer, E. (**1991**). "Auditory physics. Physical principles in hearing theory. III," Phys. Rep. **203**/3, 125–231.

Eldredge, D. H. (**1975**). "Inner ear—Cochlear mechanics and cochlear potentials," in *Handbook of Sensory Physiology* (Springer-Verlag, Berlin), Vol. 5/2.

Fernández, C. (**1952**). "Dimensions of the cochlea (guinea-pig)," J. Acoust. Soc. Am. **24**, 519–523.

Gitter, A. H., and Zenner, H. P. (**1988**). "Auditory transduction steps in single inner and outer hair cells," in *Basic Issues in Hearing*, edited by H. Duifhuis, J. W. Horst, and H. P. Wit (Academic, London).

Greenwood, D. D. (**1990**). "A cochlear frequency-position function for several species—29 years later," J. Acoust. Soc. Am. **87**, 2592–2605.

Gummer, A. W., Johnstone, B. M., and Armstrong, N. J. (**1981**). "Direct measurement of basilar membrane stiffness in the guinea pig," J. Acoust. Soc. Am. **70**, 1298–1309.

Hasko, J. A., and Richardson, G. P. (**1988**). "The ultrastructural organization and properties of the mouse tectorial membrane," Hear. Res. **35**, 21–38.

Holley, M. C., and Ashmore, J. F. (**1988**). "A cytoskeletal spring in cochlear outer hair cells," Nature **335**, 635–637.

Hudspeth, A. J. (**1989**). "How the ear's work works," Nature **341**, 397–404.

Iurato, S. (**1961**). "Submicroscopic structure of the membranous labyrinth. 2. The epithelium of Corti's organ," Z. Zellforsh. **53**, 259–298.

Iurato, S. (**1962**). "Functional implications of the nature and submicroscopic structure of the tectorial and basilar membranes," J. Acoust. Soc. Am. **62**, 1386–1395.

Johnstone, B. M., Patuzzi, R., and Yates, G. K. (**1986**). "Basilar membrane measurements and the travelling wave," Hear. Res. **22**, 147–153.

Kemp, D. T. (**1978**). "Stimulated acoustic emission from within the human auditory system," J. Acoust. Soc. Am. **64**, 1386–1391.

Kolston, P. J. (**1988**). "Sharp mechanical tuning in a cochlear model without negative damping," J. Acoust. Soc. Am. **83**, 1481–1487.

Kolston, P. J., de Boer, E., Viergever, M. A., and Smoorenburg, G. F. (**1990**). "What type of forces does the cochlear amplifier produce?," J. Acoust. Soc. Am. **88**, 1794–1801.

Kros, C. J., Rugh, A., and Richardson, G. P., (**1992**), "Mechano-electrical transducer currents in hair cells of the cultured neonatal mouse cochlea," Proc. R. Soc. London Ser. B **249**, 185–193.

Lim, D. J. (**1986**). "Functional structure of the organ of Corti: A review," Hear. Res. **22**, 117–146.

Neely, S. T., and Kim, D. O. (**1986**). "A model for active elements in cochlear biomechanics," J. Acoust. Soc. Am. **79**, 1472–1480.

Olson, E. S., and Mountain, D. C. (**1991**). "*In vivo* measurement of basilar membrane stiffness," J. Acoust. Soc. Am. **89**, 1262–1275.

Pickles, J. O. (**1988**). *An Introduction to the Physiology of Hearing* (Academic, London).

L. Robles, M. A. Ruggero, and N. C. Rich (**1986**). "Basilar membrane mechanics at the base of the chinchilla cochlea. I. Input–output functions, tuning curves and response phases," J. Acoust. Soc. Am. **80**, 1364–1374.

Ruggero, M. A., and Rich, N. C. (**1991**). "Furosemide alters organ of Corti mechanics: evidence for feedback of outer hair cells upon the basilar membrane," J. Neurosci. **11** (4), 1057–1067.

Russell, I. J., Cody, A. R., and Richardson, G. P. (**1986**). "The response of inner and outer hair cells in the basal turn of the guinea-pig cochlea and in the mouse cochlea grown in vitro," Hear. Res. **22**, 199–216.

Sellick, P. M., Patuzzi, R., and Johnstone, B. M. (**1982**). "Measurement of basilar membrane motion in the guinea pig using the Mössbauer technique," J. Acoust. Soc. Am. **72**, 131–141.

Sellick, P. M., Yates, G. K., and Johnstone, B. M. (**1983**). "The influence of Mössbauer source size and position on phase and amplitude measurements of the guinea pig basilar membrane," Hear. Res. **10**, 101–108.

Steel, K. P. (**1986**). "Tectorial membrane," in *Neurobiology of Hearing: the Cochlea*, edited by R. A. Altschuler, D. W. Hoffman, and R. P. Bobbin (Raven, New York), pp. 139–147.

Steele, C. R., and Taber, L. A. (**1979**). "Comparison of WKB and finite difference calculations for a two-dimensional cochlear model," J. Acoust. Soc. Am. **65**, 1001–1006.

Strelioff, D., and Flock, Å. (**1984**). "Stiffness of sensory-cell hair bundles in the isolated guinea pig cochlea," Hear. Res. **15**, 19–28.

Strelioff, D., Flock, Å., and Minser, K. E. (**1985**). "Role of inner and outer hair cells in mechanical frequency selectivity of the cochlea," Hear. Res. **18**, 169–175.

Tritton, D. J. (**1977**). *Physical Fluid Dynamics* (Van Nostrand Reinhold, Wokingham, United Kingdom).

Voldřich, L. (**1983**). "Experimental and topographic morphology in cochlear mechanics," in *Mechanics of Hearing*, edited by E. de Boer and M. A. Viergever (Delft U.P., Delft, The Netherlands).

Wilson, J. P. (**1980**). "Evidence for a cochlear origin for acoustic re-emission, threshold fine structure and tonal tinnitus," Hear. Res. **2**, 233–252.

Zwicker, E. (**1986**). "A hardware cochlear nonlinear preprocessing model with active feedback," J. Acoust. Soc. Am. **80**, 146–153.

Zwislocki, J. J., Chamberlain, S. C., and Slepecky, N. B. (**1988**). "Tectorial membrane I: Static mechanical properties in vivo," Hear. Res. **33**, 207–222.